metals

MDPI

Article

Si-Al-N-O Multi-Layer Coatings with Increased Corrosion Resistance Deposited on Stainless Steel by Magnetron Sputtering

Tamara Dorofeeva [1], Tatiana Gubaidulina [1], Victor Sergeev [1,2] and Marina Fedorischeva [1,*]

[1] Institute of Strength Physics and Materials Science, SB RAS, 634055 Tomsk, Russia; dorofeeva@ispms.tsc.ru (T.D.); goub2002@mail.ru (T.G.); vs@ispms.tsc.ru (V.S.)
[2] Department of Materials Science, National Research Tomsk Polytechnic University, 634050 Tomsk, Russia
* Correspondence: fed_mv@mail.ru; Tel.: +79-627-763-406

Abstract: This work studies single-layer (Al-Si-N) and multi-layer (Al-Si-N-O/Al-Si-O) coatings deposited by magnetron sputtering on stainless steel specimens (AISI 321), which can be used under aggressive conditions. The multi-layer coating consists of six alternating layers of Al-Si-N-O and Al-Si-O with a thickness of 0.9 μm and 0.2 μm, respectively. The structural-phase state and the chemical composition of the coatings were studied by transmission and scanning electron microscopy and XPS analysis. It was revealed that single-layer coatings are nanocrystalline and contain AlN and α-Si3N4 phases. Multi-layer coatings (Al-Si-N-O/Al-Si-O) are amorphous in each of the layers. The corrosion properties of substrate and coated specimens were investigated using a potentiostat in the 3.5 mg/l sea salt solution. It was found that corrosion resistance of stainless steel specimens with multi-layer coating is substantially (tenfold) higher compared with substrates and the specimens with single-layer coating.

Keywords: multi-layer coatings; magnetron sputtering; stainless steel; corrosion resistance

check for updates

Citation: Dorofeeva, T.; Gubaidulina, T.; Sergeev, V.; Fedorischeva, M. Si-Al-N-O Multi-Layer Coatings with Increased Corrosion Resistance Deposited on Stainless Steel by Magnetron Sputtering. *Metals* **2022**, *12*, 254. https://doi.org/10.3390/met12020254

Academic Editor: Wislei Riuper Osório

Received: 23 December 2021
Accepted: 27 January 2022
Published: 28 January 2022

Publisher's Note: MDPI stays neutral with regard to jurisdictional claims in published maps and institutional affiliations.

Copyright: © 2022 by the authors. Licensee MDPI, Basel, Switzerland. This article is an open access article distributed under the terms and conditions of the Creative Commons Attribution (CC BY) license (https://creativecommons.org/licenses/by/4.0/).

1. Introduction

Metal construction and manufactured parts experience complex external loads during their operation, as they suffer from atmospheric factors, aggressive substances and temperature fluctuation-induced loads. A major condition for the durability and operation reliability of structural materials is high corrosion resistance [1,2]. Stainless steels are widely used as a construction material due to their corrosion resistance under a wide range of operation conditions. However, under certain conditions stainless steel materials may need coatings, since they—like other parts made from construction steels—suffer from corrosion and consequent fracture under aggressive conditions [1–3]. Steel corrosion is a grave industrial problem which economic and ecological consequences are known well [4]. The problem of increased corrosion resistance of stainless steels can be solved by alloying steel [5–9] or using corrosion-resistant coatings. Authors have proposed various materials [10–15], ranging from metal to ceramic as coatings. Coatings provide additional protection to metal surfaces and serve as a barrier to prevent contact with chemical compounds and corrosion-inducing materials. Coatings protect metal parts from destruction during wetting, salt deposition, oxidation and from the impact of various negative environmental and industrial factors. Anti-corrosion coatings provide maximum life of metal materials (along with such physicomechanical properties as wear resistance, adhesion, hardness, thermal stability) and widen their application range [10–16].

There are numerous methods to deposit such multifunctional coatings, such as electrochemical methods [17–19], thermal methods [20], sol-gel methods [21,22] or a combination of methods [23]. In our work, we used magnetron deposition which allows forming single- and multi-layer coatings with specific functional properties. Works [24,25] show that the

most preferable coatings are multi-layer composite coatings that reduce bubble formation and delamination of a material when exposed to a corrosive environment. In addition, multi-layer composite coatings provide more heterogeneous interfaces which reduce the grain sizes and residual stresses under load [26,27].

Nitride ceramics Al-Si-N on a steel substrate possess high cracking resistance and thermal stability, hardness, wear resistance and increased tribomechanical properties [28–32]. The introduction of oxide intermediate Al-Si-O-based layers can increase the corrosion resistance of the coating, since the coating of this kind obtained by the authors [33] on aluminum had corrosion resistance. The ability of aluminium to form stable layers of Al_2O_3 in oxygen-containing environment is well known [6,34–36], therefore, the aluminum content in the surface layers increases the corrosion resistance of steel materials. Such layers have proven themselves in aggressive media at high temperatures, because aluminium oxide has outstanding mechanical properties and high chemical stability at high temperatures. Silicon oxide [15,37,38] in addition to chemical stability has high hardness and strength.

The authors of [39,40] obtained Al-Si-N and Al-O-N that possess increased physicomechanical and physicochemical properties. Nevertheless, the discussion of Al-Si-N is mainly focused on the mechanical and thermal properties of the coating; there is no description of the corrosion resistance of multi-layer Al-Si-N-O/Al-Si-O coatings. By applying two layers at the same time, one can enhance the effect of each of the layers. It is known [41] that the thickness of the coating has a negative effect due to an increase in stresses as the thickness of the layer increases. Thin coatings [42] while retaining their other qualities are elastic. In addition, nanocomposite coatings, according to the authors [43,44], have a complex of enhanced physicochemical and mechanical properties. Therefore, the main goal of present work is the investigation of the corrosion resistance of multi-layer Al-Si-N/Al-Si-O coatings in comparison to single-layer Al-Si-N coatings and substrate AISI 321 stainless steel, as well as the structural-phase state of the coatings.

2. Materials and Methods

The coating was applied to AISI 321 substrates, pre-mechanically polished with diamond paste to a roughness of Ra = 0.08 ± 0.008 μm. Then, the specimens were flushed with deionized water and ultrasonically washed in ethanol to remove residual lubrication of the surface and dried at room temperature.

The coating was formed by pulse magnetron sputtering of the $AlSi_x$ composite target in a vacuum chamber. The target consisted of aluminum and 20 ÷ 22% of silicon. The pulsed magnetron sputtering method prevented the target surface to be contaminated in the reactive gas environment of argon and oxygen during the deposition of the oxide layers of the coating. The samples were placed in the vacuum installation chamber in the position opposite to the magnetron. The distance was 60 mm ± 0.1mm. Vacuum was reached in the chamber by using a backing scroll pump and a high-vacuum cryogenic pump, providing a residual gas pressure of no more than 6×10^{-4} Pa. Next, the gas mixture of nitrogen and argon was fed into the chamber, resulting in the deposition of an Al-Si-N layer. Then, without removing the samples from the vacuum chamber, the argon-nitrogen gas mixture was pumped out and the oxygen-argon gas mixture was injected, forming an Al-Si-O layer. Then the process was repeated for spraying Al-Si-N and Al-Si-O layers. Thus, a six-layer coating was obtained. The presence of oxygen in the Al-Si-N layer is due to the specifics of the process, when the oxygen which was adsorbed on the inner surface of the chamber during the formation of the Al-Si-O layer does not have time to be desorbed during the pumping time before the deposition of the Al-Si-N layer. In this case, the first layer was based on aluminium-silicon nitride Al-Si-N (it has higher adhesion to the substrate surface) [45]. The final coating consisted of three pairs of Al-Si-N- O/Al-Si-O layers. The formation modes are given in Table 1. The growth rate of the coating was ~0.83 ± 0.04 nm/s.

Table 1. The coating deposition mode.

Conditions	Al-Si-N-O Layer	Al-Si-O Layer
Reactive gas	N_2	O_2
Target	$AlSi_x$ (x = 0.20 ÷ 0.22)	
Reactive gas pressure, Pa	0.08	0.075
General gas pressure, Pa	0.25	0.25
Magnetron discharge power, kW	1.0	1.0
Frequency, kHz	100	100
Pulse duration, μs	5	5
Procedure time, min	18	6.5
Layer thickness, μm	0.9	0.2
Temperature substrate, K	573	573

Before deposition, the surface was ion-bombarded by a beam of Ar^+ (I = 15 mA) over 5 min at an acceleration voltage of 10 kV. The total thickness of the coatings was 3.3 ± 0.2 μm.

The single-layer Al-Si-N coating was formed under the same conditions. The experimental series consisted of 12 samples with and without Al-Si-N-O/Al-Si-O and Al-Si-N coatings. At the same time, four samples were placed in the vacuum chamber and three samples were selected for corrosion testing.

The coatings were studied using an LEO EVO-50XVP scanning electron microscope (Zeiss, Germany) and a JEOL JEM-2100 transmission electron microscope (JEOL Ltd., Tokyo, Japan). The microdiffraction and X-ray microanalysis modes of the JEOL-2100 microscope were used to determine the phase and chemical composition of individual structural components and local micro-regions in the coating. The analysis used cross-section foils prepared by an Ion Slicer EM-09100IS device (JEOL Ltd., Tokyo, Japan). Since the coating consisted of several layers, the thickness of each layer was measured on the specimen's cross-section.

The elemental composition of the coating was analyzed by an energy dispersive X-ray microanalysis (EDXMA) attachment for an INCA-Energy electron microscope (Oxford Instruments, High Wycombe, UK). The phase composition of the steel specimens was determined by an DRON-7 X-ray diffractometer (UED-Lab, Petersburg, Russia).

The chemical composition of the surface layers was analyzed with X-ray photoelectronic spectroscopy (XPS) on a K-Alpha-Spectrometer (Thermo Scientific, Waltham, MA, USA) using an Al Kα monochromatic X-ray source (h_ν = 1486.6 eV). The adjustment of the spectra for the curve was performed using Thermo Electron software (v. 5.938 Avantage) with interactive Shirley background subtraction.

The corrosion rate was measured by a three-electrode electrochemical cell and P40X potentiostat. Corrosion measurements were carried out in a 0.5 M NaCl solution using a three-electrode cell, where a Ag/AgCl electrode was used as a reference electrode, and stainless steel was used as an auxiliary electrode, with an area exceeding the area of the working electrode by more than 100 times (it was 400 cm^2 with an area of the working electrode of 1 cm^2). It was necessary to neglect overvoltage in current density calculations when constructing voltage dependences. Although a 0.5 mV/s rate is adopted, it is remarked that this selection has no provided substantial distortions in the polarization curves obtained [46–48]. In this sense, it is worth noted that potential scan rate has an important role in order to minimize the effects of distortion in Tafel slopes and corrosion current density analyses, as previously reported [46–49].

3. Results and Discussion

Figure 1a shows the cross-section of the surface layer of the formed multi-layer coating on the AISI 321 stainless steel. There are evident alternating layers: one with a thickness of 0.2 μm, the other one with that of 0.9 μm, totaling to 3.3 μm. Figure 1b presents the elemental composition of the coating with the element distribution along the coating depth. The image differentiates well the alternating coating layers having different chemical

composition. Al-Si-N-based layers contain about 12 at.% of silicon, 32 at.% of aluminium, 35 at% of nitrogen and 20 at.% of oxygen. Thus, the layer is an $Al_{0.32}Si_{0.12}N_{0.32}O_{0.24}$ silicon-aluminium oxynitride. In the case of Al-Si-O layer, the coating is a fairly stable oxide. This layer contains about 60 at.% of oxygen, 20 at.% of aluminium and 20 at.% of silicon, i.e., the approximate formula of the composition is $Al_{0.2}Si_{0.2}O_{0.6}$.

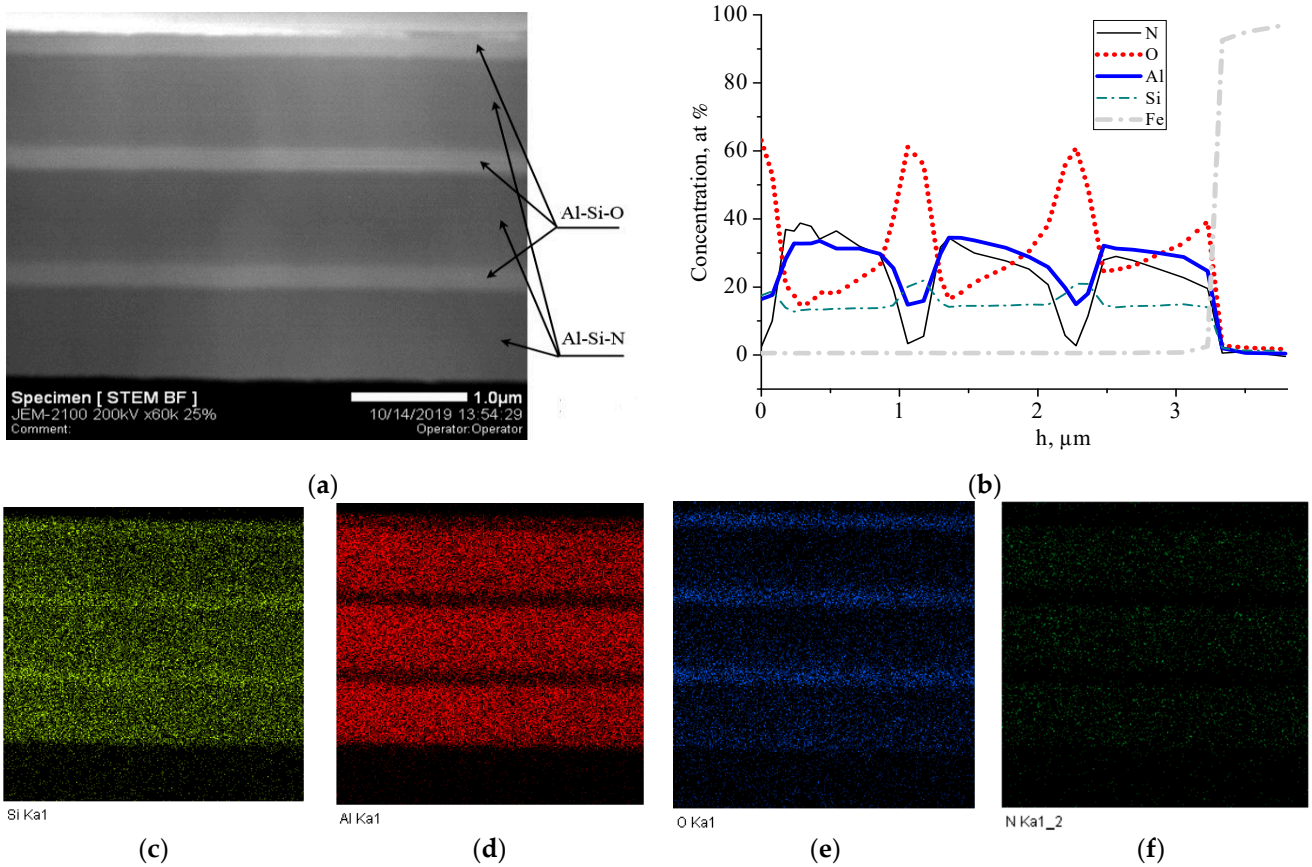
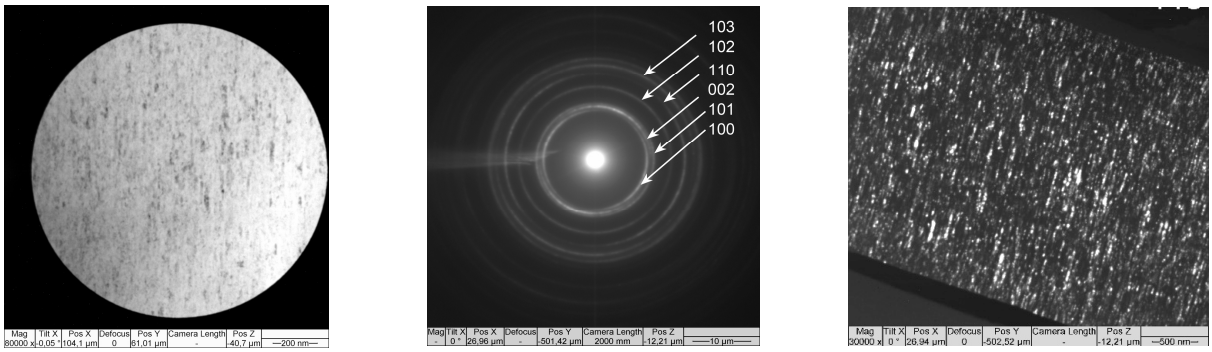


Figure 1. Transverse cross-section of the specimen with a protective coating (**a**); distribution of elements along the depth of Al-Si-N-O/Al-Si-O coating (**b**); Si distribution (**c**); Al distribution (**d**); O distribution (**e**); N distribution (**f**).

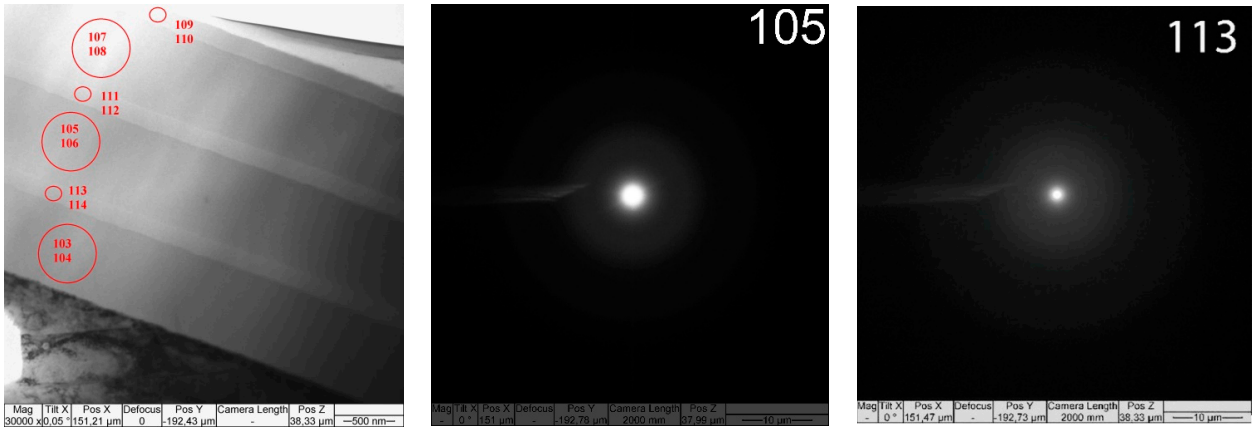
The oxygen consist in the Al-Si-N layer is due to the specifics of the process when oxygen is actively adsorbed on the surface during the Al-Si-O layer formation. The oxygen consist in the primary surface layer can be explained by two factors: the native film on the steel surface [50] associated with the absorption of atmosphere oxygen and the residual oxygen in the installation chamber, which did not have time to desorb during the pumping time before the Al-Si-N layer deposition. Oxygen, in our case, has a positive effect, which is discussed in more detail below in the article (structure, composition, corrosion mechanism).

To analyze the effect of structure on corrosion behavior of the material in more detail, the structure and phase composition of single- and multi- coatings were studied. Figure 2 presents the results of TEM-investigation of the microstructure and phase composition of surface layers in the cross-section of Al-Si-N single-layer coating deposited on the stainless-steel specimen. The bright-field TEM-image of the surface layer of the coated specimen (Figure 2a) clearly shows its nanocrystalline structure. The average transverse dimensions of AlN grains in the Al-SI-N coating is less than 15 nm. The microdiffraction pattern (Figure 3b) mainly shows a system of closed rings. The microdiffraction analysis showed that in the Al-Si-N coating, the AlN aluminium nitride phase forms with hexagonal densely packed crystal lattice. These data were confirmed by the results of X-ray studies in our previous work, where the α-Si3N4 phase was identified [51].



(**a**) (**b**) (**c**)

Figure 2. TEM-image of single-layer Al-Si-N coatings cross-section on AISI 321 steel specimen: (**a**) bright-field image; (**b**) microdiffraction pattern with indexing scheme; (**c**) dark-field image.



(**a**) (**b**) (**c**)

Figure 3. TEM-image of multi-layer Al-Si-N-O /Al-Si-O coating cross-section (**a**); microdiffraction patterns of Al-Si-N (**b**) and Al-Si-O (**c**) layers.

Figure 3 shows the multi-layer coating cross-section on AISI 321 stainless steel substrate with clear substrate crystalline structure and coating structure without crystallites.

The Al-Si-N-O layer starts forming the coating on the stainless-steel substrate; the thin layer of Al-Si-O finishes the coating. Figure 3a clearly shows the interface between the coating and the substrate. Obviously, the coating fills the surface cavities, which promotes high adhesion between the coating and the substrate and, correspondingly, increases the corrosion resistance of the coating.

The microdiffraction patterns obtained by TEM for each of the layers in transverse cross-section showed halos (total absence of reflexes) (Figure 3b,c). This speaks to both layers in the multi-layer coating to have an amorphous structure. The amorphization of the oxide layer proceeds due to the incorporation of Si atoms into the crystal lattice of Al_2O_3 [27]. The nitride layer transits into amorphous state as a result of introduction of oxygen ions into its crystal lattice the small amount of which presents after the change of gas environment in the vacuum chamber, as indicated by the authors [43,52] (during the process the microstructure evolves from crystalline to nanocrystalline and then to the amorphous microstructure). This is confirmed by the investigation of the elemental composition of coating layers in the multi-layer coating cross-section by EDXMA on the transmission electron microscope (Figure 1).

Therefore, the first layer of the coating is the amorphous aluminium-silicon oxynitride. This compound possesses higher hardness as compared to conventional silicon nitride [43–56]. Products based on aluminium-silicon oxynitride are used in the conditions of high mechanical loads, thermal shock, aggressive chemical and abrasive media, which is

conditioned by their high strength, chemical stability, corrosion and thermal stability. In the case of Al-Si-O layer, the formation of aluminium silicate is possible. It can form after simultaneous synthesis of aluminium and silicon oxides in magnetron discharge plasma [57]. This is possible due to amphiprotic properties of aluminium oxide. The molecular reaction is as follows:

$$Al_2O_3 + SiO_2 = Al_2(SiO_3)_2$$

X-ray diagrams of the initial stainless-steel specimens and the steel specimen with multi-layer coating contain typical reflexes of γ-iron [51]. XRD analysis of the multi-layer coating has shown that within the measurement error, both curves almost coincide, i.e., the coating yields no diffraction reflections after irradiation by an X-ray beam. This confirms our assumption that both layers in the multi-layer coating have an amorphous structure. Since the corrosion rate decreases with decreasing total number of grain boundaries in metal, while in the amorphous material they are absent, the observed increase in the corrosion stability of steel specimens after coating deposition, especially multi-layer coatings, can be due to this reason [27].

The assumption of aluminium silicate ($Al_2(SiO_3)_2$) formation in the multi-layer coating is confirmed by the XPS analysis of the specimen surface layer (Figure 4). The layer-by-layer oxygen spectrum at 470 nm from the coating surface has revealed oxygen peak shift towards lower energies. The oxygen concentration at the surface is three times higher, as compared to internal layers, which is conditioned by its transition from the Al-Si-O layer into the Al-Si-N-O layer, which correlates with the data received by EDXMA and presented in Figure 1b.

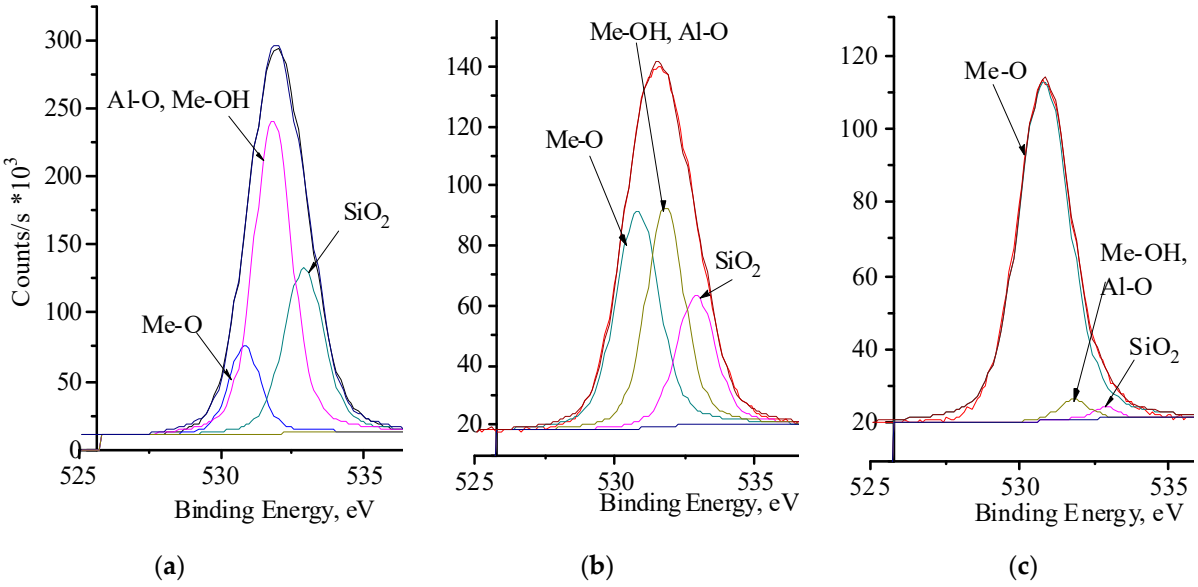


Figure 4. XPS-spectra of oxygen recorded on the stainless-steel specimen's surface with multi-layer Al-Si-N-O / Al-Si-O-coating at a depth of 0 nm (**a**), 200 nm (**b**), 300 nm (**c**).

The presence of aluminium in the coating could not be recorded as individual spectra. Oxides and hydroxides of aluminium (Al_2O_3, $Al(OH)_3$ and AlOOH) are extremely difficult to differentiate by XPS. Unfortunately, energies in spectra of aluminium oxides and hydroxides overlap each other [34]. Layer-by-layer spectra of silicon are presented in Figure 5.

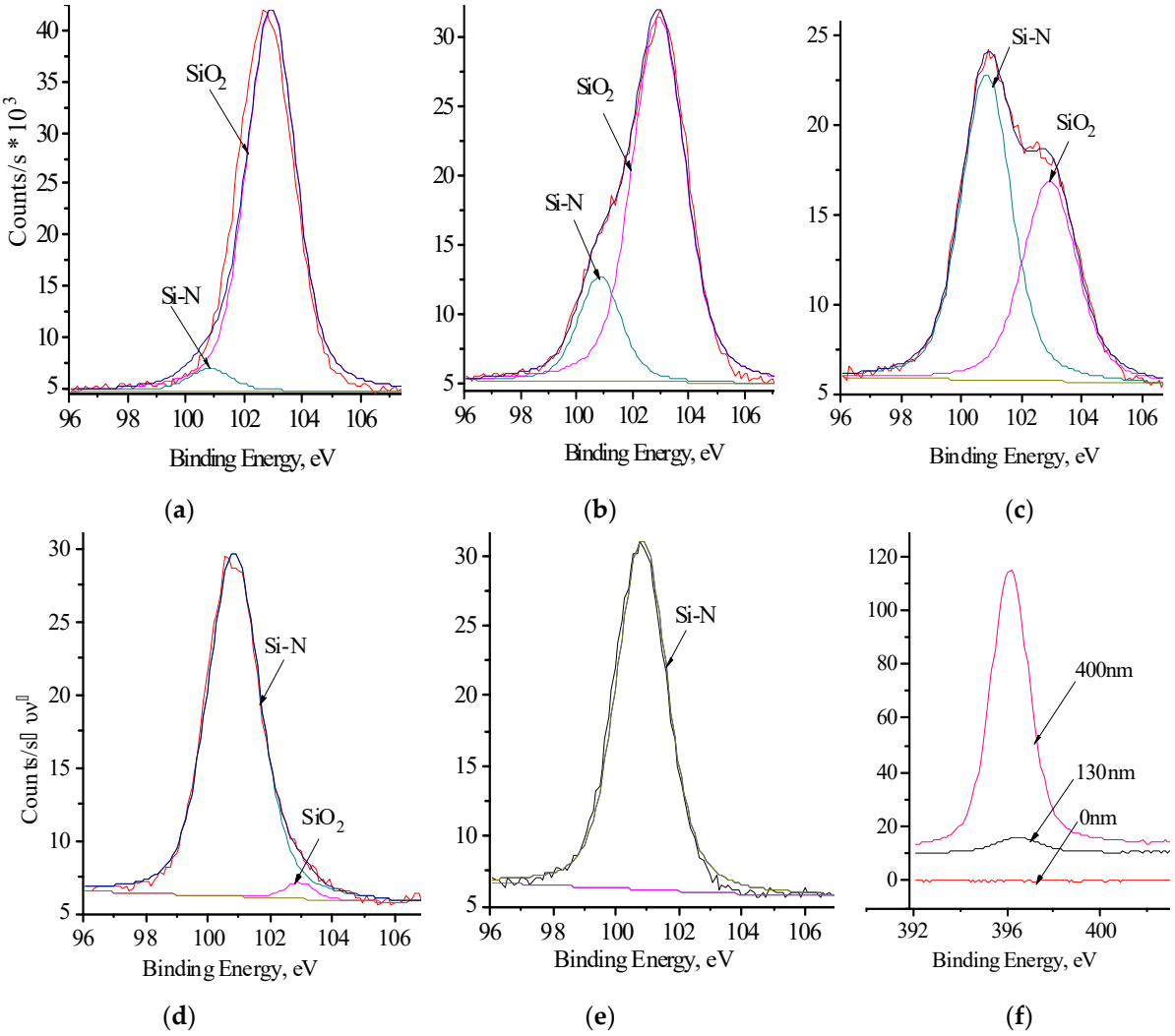


Figure 5. XPS-spectra of silicon (**a**–**e**) and nitrogen (**f**) recorded on the stainless-steel specimen's surface with multi-layer Al-Si-N-O/Al-Si-O-coating at a depth of 0 nm (**a**), 170 nm (**b**), 200 nm (**c**), 230 nm (**d**), 470 nm (**e**).

The analysis of silicon spectra has shown domination of the silicon oxide SiO_2 (E ≈ 103.1 V) on the surface; the content of Si-N (E ≈ 101 V) on the surface is negligibly small, while at a depth of ~230 nm (Figure 5d), the content of Si-N becomes substantially higher than that of its oxide. The transition layer from Al-Si-O to Al-Si-N-O can be seen in Figure 5b and 5c when silicon oxide content decreases, while that of nitride compounds conversely increases. Such data on compositions of silicon with nitrogen were confirmed after the analysis of nitrogen spectra that has shown increased nitrogen content inside the coating (Figure 5f) in its absence on the surface.

Therefore, XPS shows (Figure 4) that on the coating surface, there is aluminium oxide which is absent in deeper layers. The analysis of the silicon spectra shows that aluminium oxide is present on the surface. Then, silicon nitride forms, which becomes prevalent at a depth of 470 nm, which promotes the deposition of the layers. These data correlate with the elemental analysis data received by EDXMA.

The corrosion stability was studied on three batches of specimens: 1—without coating (three samples), 2—with single-layer Al-Si-N coating (three samples), and 3—with multi-layer Al-Si-N-O/Al-Si-O coating (three samples). To assess the corrosion resistance of the coatings, polarization curves were plotted (Figure 6). The scanning rate was 0.5 mVs^{-1}. The polarization curves were plotted using averaged values obtained for 3 similar specimens. The voltammetric curves of the coated specimens displace to the region of higher voltage

and lower current density. The polarization characteristics of the specimens with Al-Si-N coating are initially similar to those of multi-layer coating; however, the polarization potential E of the specimens with Al-Si-N-O/Al-Si-O is higher and amounts to 375 mV, unlike the single-layer coating, where E = 63 mV, while the current density is appreciably lower. The corrosion current are I_{corr} ~8.7×10^{-6} A, ~5.2×10^{-5} A and ~7.8×10^{-5} A for Al-Si-N-O/Al-Si-O, Al-Si-N and stainless-steel, respectively. Moreover, there is no passivation region for the single-layer coating. For Al-Si-N-O/Al-Si-O specimens, the passivation region lies within 700–1250 mV. In this interval, the metal surface shifts to inactive passive state due to corrosion-preventing compounds. In our case, it included the formation of oxynitrides that were identified in the Al-Si-N-based coatings (shown below).

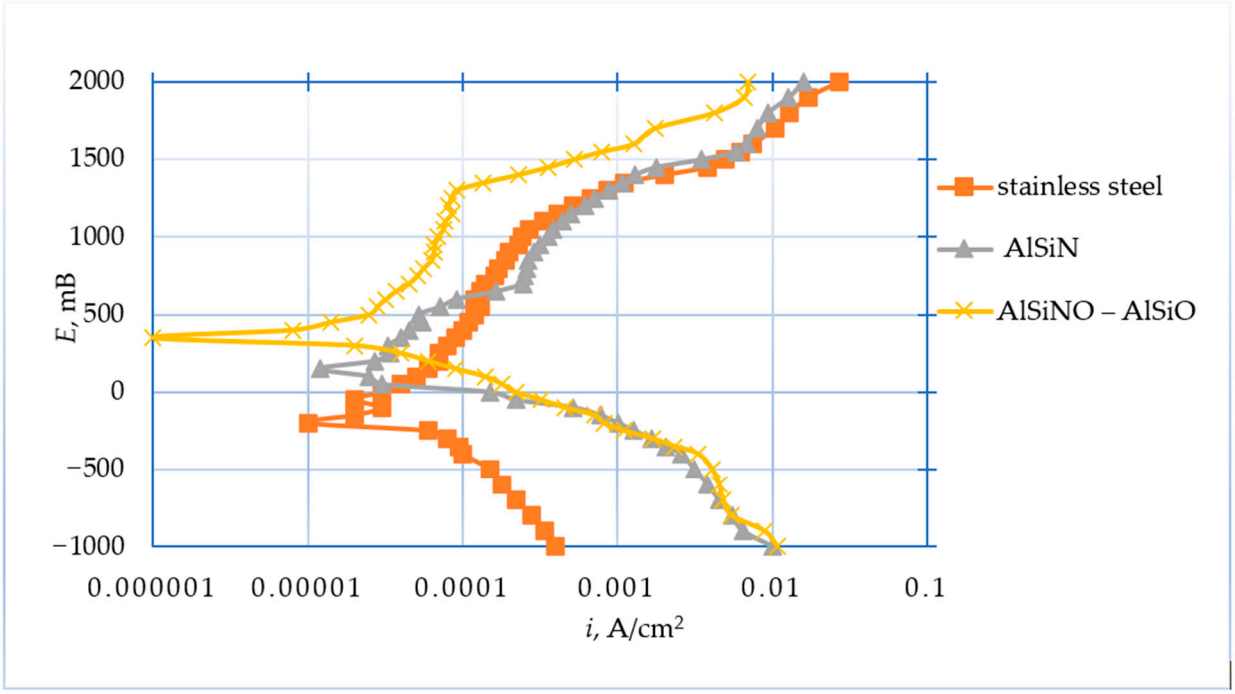
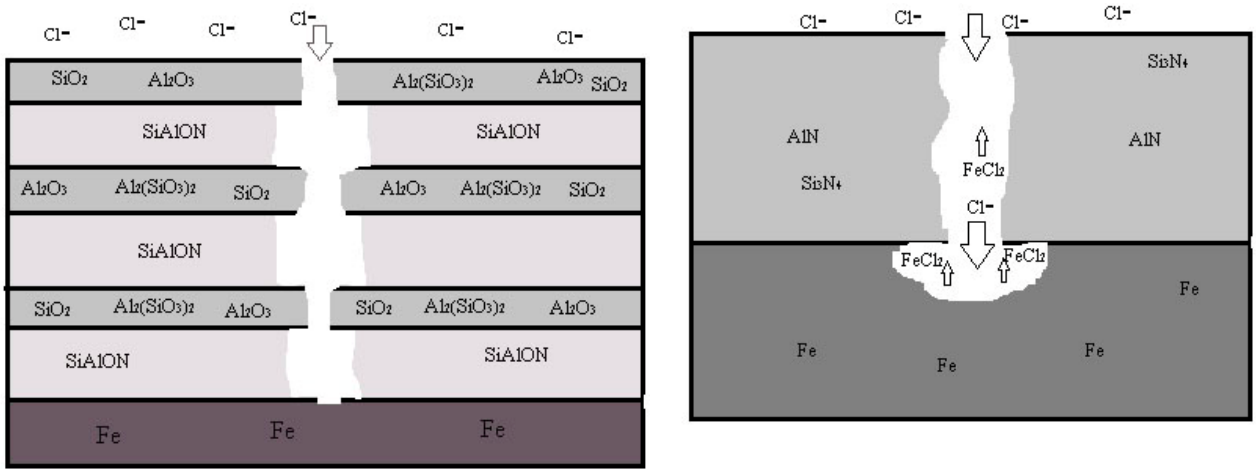


Figure 6. Potentiodynamic polarization curves of uncoated stainless-steel, Al-Si-N and Al-Si-N-O/Al-Si-O-coated specimens.

All these factors testify to increased corrosion resistance of stainless-steel specimens with Al-Si-N and Al-Si-N-O/Al-Si-O coatings, which ultimately increases for the multi-layer coating, as compared to uncoated specimens.

Multi-layer coatings surpasses single-layer coatings in terms of decreased pore and decreased defect dimensions in every layer. The formation of interfaces between heterogeneous layers inhibits the columnar crystallites growth in the coating, which may inhibit the diffusion of atoms along the coating thickness and, correspondingly, impede corrosion processes. The increase in the number of layers may increase the effect. Therefore, the multiple layers of a coating may be a positive factor decreasing corrosion of steel specimens [15,25,26]. The authors [43,53–56] consider that nanocomposite coatings have undeniable advantages due to the nanostructuring of the applied coatings. Multi-layer coatings [58] create an additional barrier. This is explained by the fact that, due to the different chemical composition of each of the layers, barriers arise that prevent the development of a leading channel for the corrosive environment penetration (Figure 7). Single-layer coatings have more defects [7,59], which may be caused by the intergranular space instability [60]. Also, it may be caused by the development of cracks in the monolithic coating as a result of additional mechanical action. Or it may be caused by the active diffusion of chlorine and/or oxygen ions, coating dissolution, and the corrosion products diffusion [8,56]. The authors

point out [41] that in such coatings, multiple channels for the penetration of a corrosive environment, and even pitting destruction of the base under the coating, often occur.



(**a**) (**b**)

Figure 7. Scheme of material behavior in an aggressive environment with chlorine anions: (**a**) multi-layer coating Al-Si-N–O/Al-Si-O, and (**b**) single-layer Al-Si-N coating.

The scheme of the mechanism of material behavior with multi- and single-layer coating after its placement into an aggressive environment containing chlorine anion (sea salt solution) is shown in Figure 7.

Regarding the impact of the aggressive environment on the steel substrate with multi-layer coating, chlorine ions—before oxidation—have to pass six dense amorphous layers, three of which contain silicon and aluminium oxides (or synthesized silicon or aluminium silicate) which are corrosion-resistant agents, while the three remaining layers contain corrosion-resistant silicon-aluminium oxynitride (Figure 7a). The presence of such corrosion resistance is confirmed by the polarization curves having passivation region. In the case of single-layer crystalline coating (following earlier works [61]) containing silicon and aluminium nitrides, chlorine ions more easily penetrate to the metal substrate forming iron chlorides, which is confirmed by the absence of the passivation region on polarization curve. We assume that the oxidant penetrates along the intercrystalline void promoting further active damage to the material under the coating (Figure 7b) with its consequent delamination and disintegration. The polarization curves for single-layer coatings presented above confirm this, i.e., while for the initial period, there is a bias towards positive potentials, the following parts of the curves for single-layer coatings and for steel substrate coincide.

4. Conclusions

Magnetron sputtering allowed producing corrosion-resistant single-layer Al-Si-N-coatings and multi-layer Al-Si-N-O/Al-Si-O-coatings. We have then examined the structural-phase state and corrosion properties of the coatings. Electron microscopy made it possible to establish that the single-layer Al-Si-N-coating is a nanocrystalline material that contains AlN phases with hexagonal densely packed crystal lattice and α-Si_3N_4 phases. The multi-layer Al–Si–O–N-based coating consists of alternating layers of Al-Si-N and Al-Si-O that have a structure close to amorphous one. Moreover, it should be noted that the coating growth conditions are the same in both cases, i.e., oxygen affects the structure of the coating.

The distribution of elements along the depth of Al-Si-N-O/Al-Si-O-coating obtained by the EDXMA method indicates that the layer of Al-Si-N-coating is an oxynitride that possesses both increased mechanical properties and enhanced corrosion resistance.

It was established that multi-layer Al-Si-N-O/Al-Si-O-coating has higher corrosion resistance vs substrate steel and single-layer Al-Si-N-layer, which is confirmed by the

polarization curves demonstrating their higher polarization potential as compared to the uncoated specimens and an order of magnitude lower value of the current density for a multi-layer coating, and hence the dissolution rate. The increased corrosion stability of Al-Si-N-O/Al-Si-O multi-layer coating is connected with first, decreased total number of grain boundaries in metal and transition from crystalline state to nanocrystalline and further amorphous state. Second, Al-Si-N-based layer in multi-layer coating is represented by $Al_{0.32}Si_{0.12}N_{0.32}O_{0.24}$ silicon-nitrogen oxynitride which has higher corrosion resistance. Third, the multi-layer coating surpasses single-layer coatings in terms of decreased pore and defect dimensions in every layer. The formation of interfaces between heterogeneous layers inhibits the growth of columnar crystallites in the coating, which may inhibit the diffusion of atoms along the coating thickness and, correspondingly, impede corrosion processes.

In our case, a synergistic effect is manifested due to several factors: there are six layers in the coating; coating is in the form of thin films; each of the layers has the amorphous structure; layers of different chemical composition alternate; the films contain the corrosion-resistant components [62].

Author Contributions: Conceptualization, V.S. and T.D.; methodology, T.D.; validation, V.S. and M.F.; investigation, T.D. and T.G.; resources, V.S.; data curation, T.D. and T.G.; writing—original draft preparation, T.D.; writing—review and editing, T.D. and M.F.; funding acquisition, V.S. All authors have read and agreed to the published version of the manuscript.

Funding: This research was performed under the government statement of work for ISPMS Project No FWRW-2021-0003, as well as its part was performed by Tomsk Polytechnic University development Program.

Institutional Review Board Statement: Not applicable.

Informed Consent Statement: Not applicable.

Data Availability Statement: Not applicable.

Conflicts of Interest: The authors declare no conflict of interest.

References

1. Chen, B.; Xu, Y.; Qu, W. Evaluation of atmospheric corrosion damage to steel space structures in coastal areas. *Int. J. Solids Struct.* **2005**, *42*, 4673–4694. [CrossRef]
2. Allam, I.M.; Maslehuddin, M.; Saricimen, H.; Al-Mana, A.I. Influence of atmospheric corrosion on the mechanical properties of reinforcing steel. *Constr. Build. Mater.* **1994**, *8*, 35–41. [CrossRef]
3. Hou, W.; Liang, C. Atmospheric Corrosion Prediction of Steels. *Corrosion* **2004**, *60*, 313–322. [CrossRef]
4. Cowell, D.; Apsimon, H. Estimating the cost of damage to buildings by acidifying atmospheric pollution in Europe. *Atmosp. Environ.* **1996**, *30*, 2959–2968. [CrossRef]
5. Luo, H.; Li, Z.; Mingers, A.M.; Raabe, D. Corrosion behavior of an equiatomic CoCrFeMnNi high-entropy alloy compared with 304 stainless steel in sulfuric acid solution. *Corros. Sci.* **2018**, *134*, 131–139. [CrossRef]
6. Li, Y.; Nie, J.; Liang, Z.; Bai, P.; Yang, Y.; Chen, B.; Liu, S.; Guan, Q.; Cai, J. Microstructure evolution and high-temperature oxidation behavior of FeCrAlNbNi alloyed zone prepared by laser surface alloying on 304 stainless steel. *J. Alloy. Compd.* **2021**, *888*, 161468. [CrossRef]
7. Nascimento, C.B.; Donatus, U.; Ríos, C.T.; Antunes, R.A. Electronic properties of the passive films formed on CoCrFeNi and CoCrFeNiAl high entropy alloys in sodium chloride solution. *J. Mater. Res. Technol.* **2020**, *9*, 13879–13892. [CrossRef]
8. Shi, Y.; Yang, B.; Xie, X.; Brechtl, J.; Dahmen, K.A.; Liaw, P.K. Corrosion of Al CoCrFeNi high-entropy alloys: Al-content and potential scan-rate dependent pitting behavior. *Corros. Sci.* **2017**, *119*, 33–45. [CrossRef]
9. Bender, R.; Schütze, M. The role of alloying elements in commercial alloys for corrosion resistance in oxidizing-chloridizing atmospheres. Part I: Literature evaluation and thermodynamic calculations on phase stabilities. *Mater. Corros.* **2003**, *54*, 567–586. [CrossRef]
10. Gawel, R.; Kyzioł, K.; Jurasz, Z.; Grzesik, Z. Oxidation resistance of valve steels covered with thin SiC coatings, obtained by RF CVD. *Corros. Sci.* **2018**, *145*, 16–25. [CrossRef]
11. Szymański, K.; Hernas, A.; Moskal, G.; Myalska, H. Thermally sprayed coatings resistant to erosion and corrosion for power plant boilers—A review. *Surf. Coat. Technol.* **2015**, *268*, 153–164. [CrossRef]
12. Matthews, S.; James, B.; Hyland, M. High temperature erosion of Cr3C2-NiCr thermal spray coatings—The role of phase microstructure. *Surf. Coatings Technol.* **2009**, *203*, 1144–1153. [CrossRef]

13. Formanek, B.; Szymański, K.; Szczucka-Lasota, B.; Włodarczyk, A. New generation of protective coatings intended for the power industry. *J. Mater. Process. Technol.* **2005**, *164–165*, 850–855. [CrossRef]
14. Wu, Z.; Zhao, X.; Liu, Y.; Cai, Y.; Li, J.; Chen, H.; Wan, Q.; Yang, D.; Tan, J.; Liu, H.; et al. Lead-bismuth eutectic (LBE) corrosion behavior of AlTiN coatings at 550 and 600 °C. *J. Nucl. Mater.* **2020**, *539*, 152280. [CrossRef]
15. Sadeghi, E.; Markocsan, N.; Joshi, S. Advances in corrosion-resistant thermal spray coatings for renewable energy power plants. Part I: Effect of composition and microstructure. *J. Therm. Spray Technol.* **2019**, *28*, 1749–1788. [CrossRef]
16. Zhang, Z.; Tang, J.; Wang, Y.; Wang, H.; Normand, B.; Zuo, Y. Electrodeposition of a Pd-Ni/TiO2 composite coating on 316L SS and its corrosion behavior in hot sulfuric acid solution. *Coatings* **2018**, *8*, 182. [CrossRef]
17. Jiang, L.; Syed, J.A.; Gao, Y.; Lu, H.; Meng, X. Electrodeposition of $Ni(OH)_2$ reinforced polyaniline coating for corrosion protection of 304 stainless steel. *Appl. Surf. Sci.* **2018**, *440*, 1011–1021. [CrossRef]
18. Zhang, L.; Liu, S.; Han, H.; Zhou, Y.; Hu, S.; He, C.; Yan, Q. Studies on the formation process and anti-corrosion performance of polypyrrole film deposited on the surface of Q235 steel by an electrochemical method. *Surf. Coatings Technol.* **2018**, *341*, 95–102. [CrossRef]
19. Fotovvati, B.; Namdari, N.; Dehghanghadikolaei, A. On coating techniques for surface protection: A review. *J. Manuf. Mater. Process.* **2019**, *3*, 28. [CrossRef]
20. Zand, R.Z.; Verbeken, K.; Adriaens, A. The corrosion resistance of 316L stainless steel coated with a silane hybrid nanocomposite coating. *Prog. Org. Coat.* **2011**, *72*, 709–715. [CrossRef]
21. Akhtar, S.; Matin, A.; Kumar, A.M.; Ibrahim, A.; Laoui, T. Enhancement of anticorrosion property of 304 stainless steel using silane coatings. *Appl. Surf. Sci.* **2018**, *440*, 1286–1297. [CrossRef]
22. Dorofeeva, T.I.; Gubaidullina, T.A.; Gritsenko, B.P.; Sergeev, V.P. Structural phase state and thermal cyclic stability of the thermal barrier Zr-Si-O coatings deposited on a copper substrate by the microplasma method. *Prot. Met. Phys. Chem. Surf.* **2019**, *55*, 695–699. [CrossRef]
23. Salem, A.A.; Grgur, B.N. The influence of the polyaniline initial oxidation states on the corrosion of steel with composite coatings. *Prog. Org. Coat.* **2018**, *119*, 138–144. [CrossRef]
24. Sambyal, P.; Ruhi, G.; Dhawan, S.; Bisht, B.; Gairola, S. Enhanced anticorrosive properties of tailored poly(aniline-anisidine)/chitosan/SiO_2 composite for protection of mild steel in aggressive marine conditions. *Prog. Org. Coat.* **2018**, *119*, 203–213. [CrossRef]
25. Zhang, D.; Qi, Z.; Wei, B.; Wu, Z.; Wang, Z. Anticorrosive yet conductive Hf/Si_3N_4 multilayer coatings on AZ91D magnesium alloy by magnetron sputtering. *Surf. Coa Technol.* **2017**, *309*, 12–20. [CrossRef]
26. Escobar, C.; Villarreal, M.; Caicedo, J.; Aperador, W.; Prieto, P. Novel performance in physical and corrosion resistance HfN/VN coating system. *Surf. Coat. Technol.* **2013**, *221*, 182–190. [CrossRef]
27. Musil, J.; Remnev, G.; Legostaev, V.; Uglov, V.; Lebedynskiy, A.; Lauk, A.; Procházka, J.; Haviar, S.; Smolyanskiy, E. Flexible hard Al-Si-N films for high temperature operation. *Surf. Coat. Technol.* **2016**, *307*, 1112–1118. [CrossRef]
28. Liu, H.; Tang, W.; Hui, D.; Hei, L.; Lu, F. Characterization of (Al, Si)N films deposited by balanced magnetron sputtering. *Thin Solid Films* **2009**, *517*, 5988–5993. [CrossRef]
29. Chang, C.-L.; Huang, C.-S. Effect of bias voltage on microstructure, mechanical and wear properties of Al-Si-N coatings deposited by cathodic arc evaporation. *Thin Solid Films* **2011**, *519*, 4923–4927. [CrossRef]
30. Sergeev, V.P.; Panin, V.E.; Rizakhanov, R.N.; Koroteev, A.S.; Fedorischeva, M.V.; Neufeld, V.V.; Kalashnikov, M.P. Thermal cycle durability of heat-shielding coatings on the basis of Zr-Y-O/Si-Al-N under ion treatment of copper substrates. *Adv. Mater. Res.* **2014**, *880*, 146–150. [CrossRef]
31. Ho, W.Y.; Tsai, C.H.; Hsu, C.H. Corrosion behavior of CrN/AlSiN multilayer coatings on AISI 304 stainless steel in aluminum alloy melt. *Adv. Mater. Res.* **2011**, *415–417*, 1938–1941. [CrossRef]
32. Voevodin, A.; Yerokhin, A.; Lyubimov, V.; Donley, M.; Zabinski, J. Characterization of wear protective Al-Si-O coatings formed on Al-based alloys by micro-arc discharge treatment. *Surf. Coat. Technol.* **1996**, *86–87*, 516–521. [CrossRef]
33. Arevalo, J.L.M.; Perez-Trujillo, F.J.; Castañeda, S.I. Aluminum-silicon coatings on austenitic stainless steel (AISI 304 and 317) deposited by chemical vapor deposition in a fluidized bed. *Ingeniería e Investigación* **2014**, *34*, 5–10. [CrossRef]
34. Zhao, Z.; Lu, J.; Huang, J.; Wang, Q.; Zhang, X.; Wang, J. A comprehensive investigation of phase evolution of Al-Si coating during the prolonged aging at 650 °C. *Corros. Sci.* **2021**, *189*, 109605. [CrossRef]
35. Gao, M.; Lu, W.; Yang, B.; Zhang, S.; Wang, J. High corrosion and wear resistance of Al-based amorphous metallic coating synthesized by HVAF spraying. *J. Alloys Compd.* **2018**, *735*, 1363–1373. [CrossRef]
36. Castañeda, S.; Perez-Trujillo, F.J. Al-Mn CVD-FBR coating on P92 steel as protection against steam oxidation at 650 °C: TGA-MS study. *J. Nucl. Mater.* **2018**, *499*, 419–430. [CrossRef]
37. Fu, G.; Wu, Y.; Liu, Q.; Li, R.; Su, Y. Hot corrosion behavior of stainless steel with Al-Si/Al-Si-Cr coating. *High Temp. Mater. Process.* **2016**, *36*, 243–248. [CrossRef]
38. Musil, J.; Šašek, M.; Zeman, P.; Čerstvý, R.; Heřman, D.; Han, J.; Šatava, V. Properties of magnetron sputtered Al–Si–N thin films with a low and high Si content. *Surf. Coat. Technol.* **2008**, *202*, 3485–3493. [CrossRef]
39. Musil, J.; Jílek, R.; Meissner, M.; Tölg, T.; Čerstvý, R. Two-phase single layer Al-O-N nanocomposite films with enhanced resistance to cracking. *Surf. Coat. Technol.* **2012**, *206*, 4230–4234. [CrossRef]

40. Zhang, D.; Guo, L.; Duan, L.; Tuan, W.-H. Preparation of Cr-based multilayer coating on stainless steel as bipolar plate for PEMFCs by magnetron sputtering. *Int. J. Hydrogen Energy* **2011**, *36*, 2184–2189. [CrossRef]
41. Ye, Y.; Liu, Z.; Liu, W.; Zhang, D.; Wang, Y.; Zhao, H.; Wang, L.; Li, X. Bias design of amorphous/nanocrystalline Cr Al Si N films for remarkable anti-corrosion and anti-wear performances in seawater. *Tribol. Int.* **2018**, *121*, 410–419. [CrossRef]
42. Pélisson, A.; Parlinska-Wojtan, M.; Hug, H.; Patscheider, J. Microstructure and mechanical properties of Al-Si-N transparent hard coatings deposited by magnetron sputtering. *Surf. Coat. Technol.* **2007**, *202*, 884–889. [CrossRef]
43. Pélisson-Schecker, A.; Hug, H.J.; Patscheider, J. Morphology, microstructure evolution and optical properties of Al-Si-N nanocomposite coatings. *Surf. Coat. Technol.* **2014**, *257*, 114–120. [CrossRef]
44. Rajendran, S.; Nguyen, T.A.; Kakooei, S.; Yeganeh, M.; Li, Y. *Corrosion Protection at the Nanoscale*; Elsevier: Amsterdam, The Netherlands, 2020; p. 526. [CrossRef]
45. Gritsenko, B.P.; Rechenko, D.S.; Rogachev, E.A.; Smyrnova, K.V.; Bagdasaryan, A.A.; Sergeev, V.P.; Popov, A.Y.; Nogaibekova, G.Z.; Fedorischeva, M.V.; Pogrebnjak, A.D. Enhancement of the wear resistance of tungsten cobalt carbide plates using ion implantation and Al-Si-N coatings. In *Springer Proceedings in Physics*; Springer: Singapore, 2020; Volume 240, pp. 279–286. [CrossRef]
46. Meyer, Y.A.; Bonatti, R.S.; Bortolozo, A.D.; Osório, W.R. Electrochemical behavior and compressive strength of Al-Cu/xCu composites in NaCl solution. *J. Solid State Electrochem.* **2021**, *25*, 1303–1317. [CrossRef]
47. Osório, W.R.; Freitas, E.S.; Garcia, A. EIS and potentiodynamic polarization studies on immiscible monotectic Al-In alloys. *Electrochim. Acta* **2013**, *102*, 436–445. [CrossRef]
48. Zhang, X.L.; Jiang, Z.H.; Yao, Z.P.; Song, Y.; Wu, Z.D. Effects of scan rate on the potentiodynamic polarization curve obtained to determine the Tafel slopes and corrosion current density. *Corros. Sci.* **2009**, *51*, 581–587. [CrossRef]
49. McCafferty, E. Validation of corrosion rates measured by the Tafel extrapolation method. *Corros. Sci.* **2005**, *47*, 3202–3215. [CrossRef]
50. Qiu, Y.; Thomas, S.; Gupta, R.; Gengenbach, T.; Jones, R.; Birbilis, N. A surface study of the native oxide upon a compositionally complex alloy. *Corrosion* **2018**, *74*, 1312–1317. [CrossRef]
51. Dorofeeva, T.I.; Gubaidulina, T.A.; Sergeev, V.P.; Kalashnikov, M.P.; Voronov, A.V. The structural-phase composition of the magnetron-sputtered Al-Si-N-O-based coatings. *AIP Conf. Proc.* **2020**, *2310*, 020076. [CrossRef]
52. Fischer, M.; Trant, M.; Thorwarth, K.; Crockett, R.; Patscheider, J.; Hug, H.J. Understanding the microstructural evolution and mechanical properties of transparent Al-O-N and Al-Si-O-N films. *Sci. Technol. Adv. Mater.* **2019**, *20*, 1031–1042. [CrossRef]
53. Knotek, O.; Loffler, F.; Beele, W. PVD coating in the system SI-AL-O-N. *Key Eng. Mater.* **1994**, *89*, 275–280. [CrossRef]
54. Luo, J.; Xi, C.; Gu, Y.; Zhang, L.; Zhang, C.; Xue, Y.; Liu, R. Superplastic forging for sialon-based nanocomposite at ultralow temperature in the electric field. *Sci. Rep.* **2019**, *9*, 2452. [CrossRef] [PubMed]
55. Cao, G.Z.; Metselaar, R. α'-Sialon ceramics: A review. *Chem. Mater.* **1991**, *3*, 242–252. [CrossRef]
56. Bobzin, K.; Brögelmann, T.; Kruppe, N.; Carlet, M. Wear behavior and thermal stability of HPPMS (Al,Ti,Cr,Si)ON, (Al,Ti,Cr,Si)N and (Ti,Al,Cr,Si)N coatings for cutting tools. *Surf. Coat. Technol.* **2020**, *385*, 125370. [CrossRef]
57. Whitney, D.L. Coexisting andalusite, kyanite, and sillimanite: Sequential formation of three Al_2SiO_5 polymorphs during progressive metamorphism near the triple point. *Am. Miner.* **2002**, *87*, 405–416. [CrossRef]
58. Guzmán, P.; Aperador, W.; Yate, L. Enhancement of the pitting corrosion resistance of AISI 316LVM Steel with Ta-Hf-C/Au bilayers for biomedical applications. *J. Nanomater.* **2017**, *2017*, 6825250. [CrossRef]
59. Zhang, S.; Wu, J.; Qi, W.; Wang, J. Effect of porosity defects on the long-term corrosion behaviour of Fe-based amorphous alloy coated mild steel. *Corros. Sci.* **2016**, *110*, 57–70. [CrossRef]
60. Ye, Q.; Feng, K.; Li, Z.; Lu, F.; Li, R.; Huang, J.; Wu, Y. Microstructure and corrosion properties of CrMnFeCoNi high entropy alloy coating. *Appl. Surf. Sci.* **2017**, *396*, 1420–1426. [CrossRef]
61. Dorofeeva, T.I.; Gubaidulina, T.A.; Sergeev, V.P.; Kalashnikov, M.P.; Voronov, A.V. Change in the structure and corrosion resistance of a nickel-chrome coating on stainless steel during implantation of high energy Al+ and B+ Ions. *Sov. Phys. J.* **2020**, *63*, 1186–1194. [CrossRef]
62. Majumdar, S.; Paul, B.; Chakraborty, P.; Kishor, J.; Kain, V.; Dey, G.K. Formation of Al_2O_3 /FeAl coatings on a 9Cr-1Mo steel, and corrosion evaluation in flowing Pb-17Li loop. *J. Nucl. Mater.* **2017**, *486*, 60–65. [CrossRef]